

# A hypomorphic variant in the translocase of the outer mitochondrial membrane complex subunit TOMM7 causes short stature and developmental delay

Cameron Young,<sup>1</sup> Dominyka Batkovskyte,<sup>2</sup> Miyuki Kitamura,<sup>3</sup> Maria Shvedova,<sup>1</sup> Yutaro Mihara,<sup>4</sup> Jun Akiba,<sup>5</sup> Wen Zhou,<sup>1</sup> Anna Hammarsjö,<sup>2,6</sup> Gen Nishimura,<sup>2,7</sup> Shuichi Yatsuga,<sup>3,8</sup> Giedre Grigelioniene,<sup>2,6,9,\*</sup> and Tatsuya Kobayashi<sup>1,10,\*</sup>

## Summary

Mitochondrial diseases are a heterogeneous group of genetic disorders caused by pathogenic variants in genes encoding gene products that regulate mitochondrial function. These genes are located either in the mitochondrial or in the nuclear genome. The TOMM7 gene encodes a regulatory subunit of the translocase of outer mitochondrial membrane (TOM) complex that plays an essential role in translocation of nuclear-encoded mitochondrial proteins into mitochondria. We report an individual with a homozygous variant in *TOMM7* (c.73T>C, p.Trp25Arg) that presented with a syndromic short stature, skeletal abnormalities, muscle hypotonia, microvesicular liver steatosis, and developmental delay. Analysis of mouse models strongly suggested that the identified variant is hypomorphic because mice homozygous for this variant showed a milder phenotype than those with homozygous *Tomm7* deletion. These *Tomm7* mutant mice show pathological changes consistent with mitochondrial dysfunction, including growth defects, severe lipoatrophy, and lipid accumulation in the liver. These mice die prematurely following a rapidly progressive weight loss during the last week of their lives. *Tomm7* deficiency causes a unique alteration in mitochondrial function; despite the bioenergetic deficiency, mutant cells show increased oxygen consumption with normal responses to electron transport chain (ETC) inhibitors, suggesting that *Tomm7* deficiency leads to an uncoupling between oxidation and ATP synthesis without impairing the function of the tricarboxylic cycle metabolism or ETC. This study presents evidence that a hypomorphic variant in one of the genes encoding a subunit of the TOM complex causes mitochondrial disease.

Mitochondria are double-membrane-bound organelles that are essential for diverse cellular processes, including energy production through the process called oxidative phosphorylation (OXPHOS) and supplying a variety of bioactive metabolites.<sup>1</sup> Dysfunctions of mitochondria are associated with various human conditions such as metabolic,<sup>2</sup> neurodegenerative,<sup>3</sup> kidney,<sup>4</sup> cardiovascular,<sup>5</sup> and neuromuscular diseases.<sup>6</sup> Mitochondrial diseases can be caused by pathogenic variants in genes located in the mitochondrial genome DNA (mtDNA) or in the nuclear genome that encode mitochondrial proteins.<sup>7,8</sup>

The mitochondrion contains about 1,500 proteins in humans. Since mtDNA encodes only 13 mitochondrial proteins that are subunits of the respiratory chain complexes, the majority of mitochondrial proteins are encoded in the nuclear DNA.<sup>9</sup> These proteins are synthesized in the cytoplasm and imported into mitochondria. These nuclear DNA-encoded mitochondrial proteins localized inside of the mitochondria need to be transported through the outer mitochondrial membrane (OMM) into the intermembrane space (IMS). This process is mediated by the

translocase of the outer membrane (TOM) complex.<sup>10</sup> Adequate control of both quantity and quality of mitochondrial proteins via their synthesis, degradation, and transportation is essential for healthy cellular function, and aberration in mitochondrial proteostasis leads to mitochondrial dysfunction and diseases.<sup>11</sup>

The TOM complex consists of multiple subunits including the core proteins TOMM40, which forms a barrel structure through which mitochondrial proteins translocate from cytosolic space into IMS, and TOMM20 and TOMM22, which provide a binding interface for mitochondrial proteins by associating with their N-terminal cleavable extension, called a “pre-sequence,” that is present in a majority of nuclear-encoded mitochondrial proteins.<sup>12</sup> Three evolutionarily conserved regulatory subunits, TOMM5, -6, and -7, are directly associated with TOMM40.<sup>13,14</sup> These regulatory subunits have been suggested to modulate the assembly and stability of the TOM complex and thereby control its function.<sup>15–17</sup> In addition to the role of TOM complex assembly, TOMM7 has been implicated in regulation of mitophagy through

<sup>1</sup>Endocrine Unit, Massachusetts General Hospital and Harvard Medical School, Boston, MA 02114, USA; <sup>2</sup>Department of Molecular Medicine and Surgery, Karolinska Institutet, Stockholm 17177, Sweden; <sup>3</sup>Department of Pediatrics and Child Health, Kurume University School of Medicine, Kurume, Fukuoka 830-0011, Japan; <sup>4</sup>Department of Pathology, Kurume University School of Medicine, Kurume, Fukuoka 830-0011, Japan; <sup>5</sup>Department of Diagnostic Pathology, Kurume University Hospital, Kurume, Fukuoka 830-0011, Japan; <sup>6</sup>Department of Clinical Genetics, Karolinska University Laboratory, Karolinska University Hospital, Stockholm 17176, Sweden; <sup>7</sup>Center for Intractable Disease, Saitama Medical University Hospital, Saitama, Japan; <sup>8</sup>Department of Pediatrics, Faculty of Medicine, Fukuoka University, Fukuoka 814-0180, Japan; <sup>9</sup>Department of Clinical Genetics, and Department of Biomedical and Clinical Sciences, Linköping University, Linköping 58183, Sweden

<sup>10</sup>Lead contact

\*Correspondence: [giedre.grigelioniene@ki.se](mailto:giedre.grigelioniene@ki.se) (G.G.), [tkobayashi1@mgh.harvard.edu](mailto:tkobayashi1@mgh.harvard.edu) (T.K.)

<https://doi.org/10.1016/j.xhgg.2022.100148>.

© 2022 This is an open access article under the CC BY-NC-ND license (<http://creativecommons.org/licenses/by-nc-nd/4.0/>).



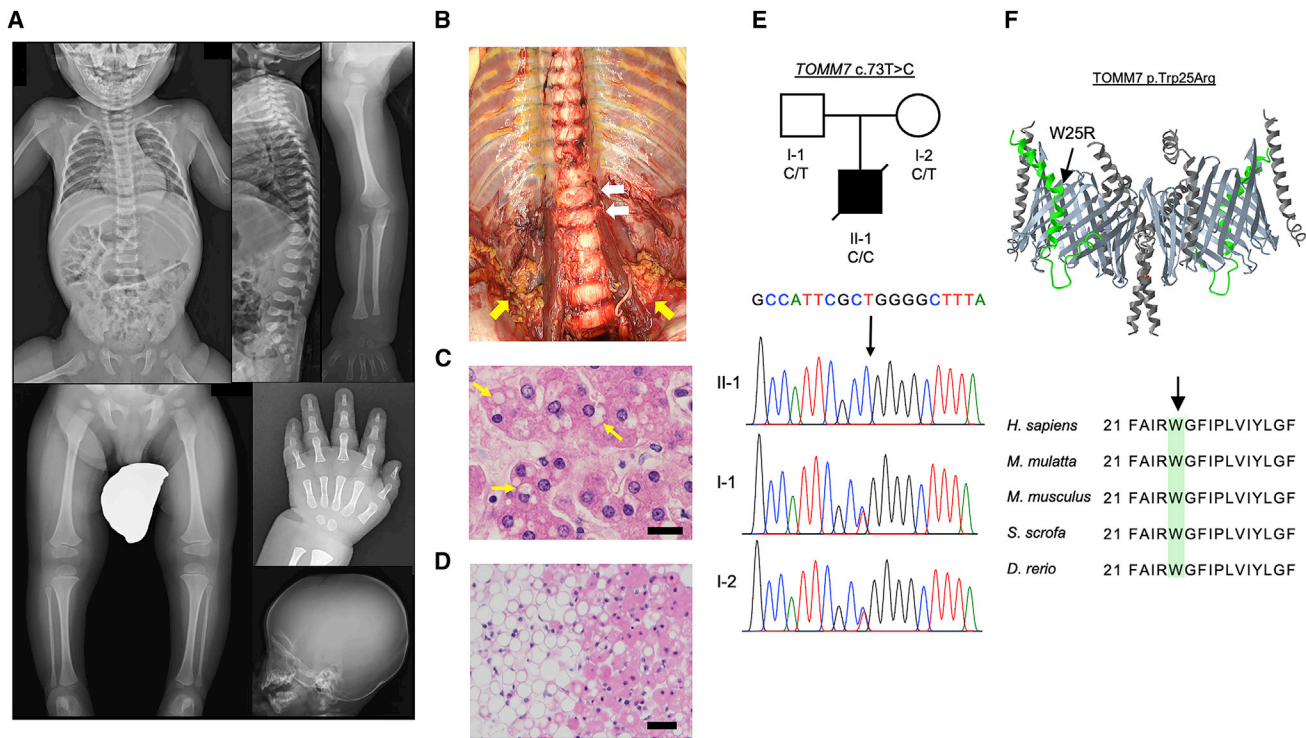


**Figure 1. A novel syndromic skeletal dysplasia associated with a *TOMM7* variant**

(A) Skeletal survey of the affected individual at the age of 1 year and 8 months. Note thin ribs, mild platyspondyly with ovoid vertebral bodies, gracile long tubular bones with relatively large epiphyses in upper and lower extremities, *coxa valga*, slender metacarpals and proximal phalanges, short middle phalanges with metaphyseal flaring of the proximal ends, and craniofacial disproportion (small facial bones).

(B) Frontal view of the spine and retroperitoneal fat tissues during autopsy. Flat and oval-shaped vertebral bodies (white arrows) and relatively prominent brown adipose tissues (yellow arrows) are shown.

(C) Hematoxylin and eosin-stained liver tissue. Yellow arrows indicate translucent intracellular vesicles in hepatocytes suggesting lipid accumulation. Scale bar, 20  $\mu$ m.

(D) Hematoxylin and eosin-stained retroperitoneal fat tissue. The size of white adipocytes (left half of the image) is relatively small (15–45  $\mu$ m in diameter) and is similar to that of brown adipocytes (right half of the image). Scale bar, 50  $\mu$ m.

(E) The pedigree of the affected individual and Sanger sequencing data for the variant. The parents are heterozygous and the proband is homozygous for *TOMM7* c.73T>C variant.

(F) Three-dimensional (3D) structure of the TOM complex dimer. TOMM7 is indicated in green color, TOMM40 barrels are in light gray. Other subunits, TOMM5, TOMM6, and TOMM22 are in dark gray. The variant residue (indicated by the arrow) is located next to the arginine residue at the position 24, which is predicted to be important for interaction with TOMM40.<sup>20</sup> The image is modified from the data (ID: 195358) of the Molecular Modeling Database.<sup>21,22</sup>

stabilization of PINK1, a crucial regulator of parkin (PARK2) that initiates mitochondrial protein degradation upon mitochondrial damage.<sup>18,19</sup> Thus far, no human diseases have been reported to be associated with variants in genes encoding TOM complex subunits. Here, we present a boy with a short stature and growth failure associated with a homozygous missense variant in *TOMM7* (MIM: 607980) and experimental evidence for its pathogenic role.

The affected individual and his healthy parents were enrolled in the study of rare congenital skeletal disorders after being diagnosed to have an unknown condition with skeletal abnormalities. The patient, a male infant, born to non-consanguineous Japanese parents, came to medical attention due to progressive growth failure. He was born via Cesarean section due to his mother's hypertension at the gestational age of 38 weeks and 5 days. His birth weight (3,240 g) and length (50 cm) were normal (Z score +0.3 and +0.06, respectively), and the routine

neonatal screening tests for congenital metabolic diseases were negative. He showed progressive postnatal growth retardation. At 1 year and 3 months of age, his body weight and height were 6,905 g (Z score –3.6) and 65.5 cm (Z score –5.4), respectively, and his arm span (61 cm) was shorter than his height (65.2 cm). Other clinical features include narrow thorax, broad hands, small nails, nystagmus, muscular hypotonia with frog-leg posture and poor head control (head raising at 6 months), tachypnea (respiratory rate 32/min), and retractive breathing. The results of his laboratory tests at 12 and 20 months showed increased serum lactate dehydrogenase (LDH) levels and moderately increased white blood cell counts (Table S1). Endocrinological test results showed normal values of thyroid hormone, thyroid-stimulating hormone, and growth hormone (Table S2). Radiology examination revealed relatively large neurocranium, underdeveloped facial bones, open anterior fontanel, mildly flat and rounded outline

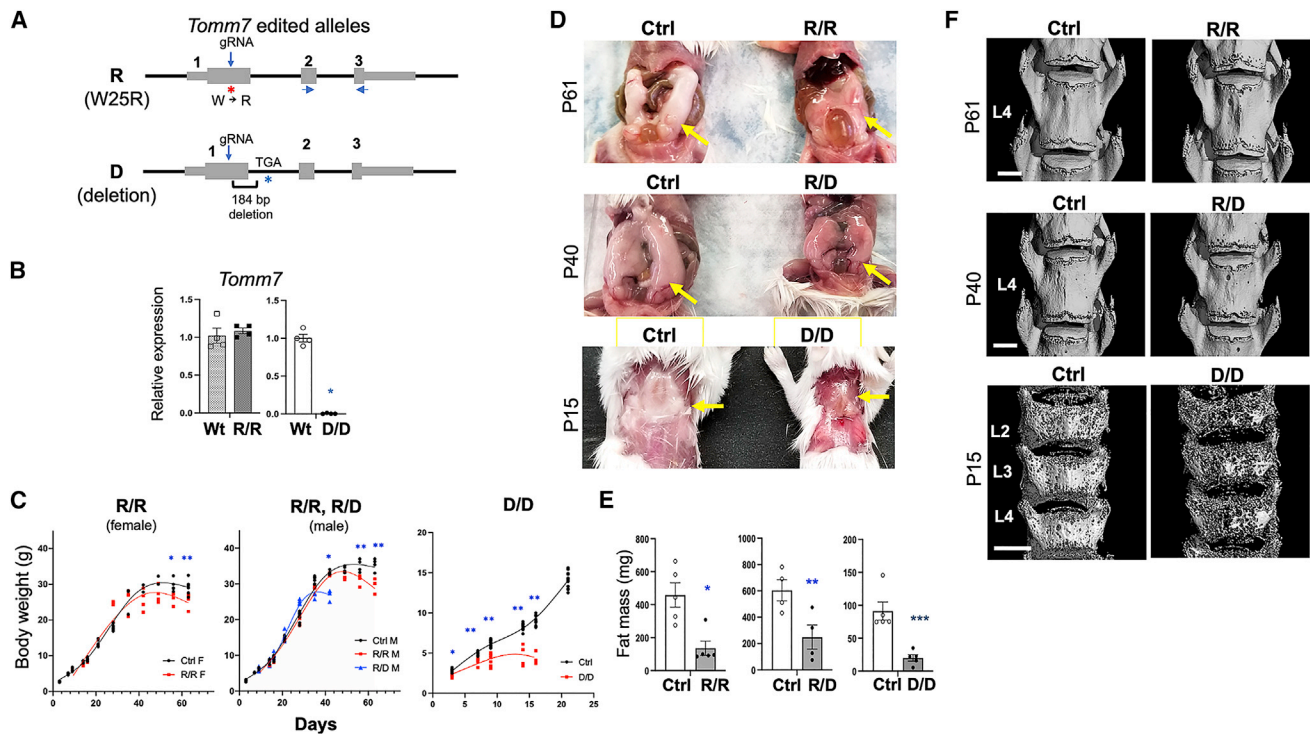


**Figure 2. Generation and gross phenotype of *Tomm7* mutant mice**

(A) Edited alleles of the mouse *Tomm7* gene in mice. Using CRISPR-mediated genome editing in mouse zygotes, a knockin (R) allele with the Trp25Arg (W25R) substitution and a deletion (D) allele missing a 184 bp sequence including the first exon-intron boundary were created. The locations of primers for qRT-PCR in (B) are indicated by arrows.

(B) qRT-PCR analysis of *Tomm7* expression in mutant mice. RNA was isolated from *Tomm7*(D/D) bone marrow stromal cells and from the liver of *Tomm7*(R/R) along with their wild-type littermate controls.  $\pm$  SEM,  $n = 4$ ,  $*p < 0.0001$ ,  $t$  test.

(C) Growth (body weight) of mice with indicated genotypes and genders. Both wild type and heterozygotes are used as control. Missing values in mutant mouse groups are due to either spontaneous death or euthanasia per IACUC protocol criteria. Left: for (D/D) mice and their control cohorts, both genders are included.  $n = 4-6$  for (D/D),  $n = 8-12$  for control (Ctrl),  $*p = 0.0041$ ,  $**p < 0.0001$ . Mann-Whitney U test. Middle: growth of male (R/R) and compound mutant (R/D) mice.  $n = 4$  for (R/R),  $n = 4$  for (R/D), and  $n = 5$  for Ctrl.  $*p = 0.0286$  (R/R) versus (R/D),  $**p = 0.0286$  Ctrl versus (R/R). Mann-Whitney U test. Right: growth of female (R/R) mice.  $n = 4$  for (R/R),  $n = 6$  for Ctrl.  $*p = 0.0159$ ,  $**p = 0.0038$ . Mann-Whitney U test.

(D) Representative images of lipoatrophy in (R/R), (R/D), and (D/D) mice at indicated ages. The dorsal white adipose tissue covering the interscapular brown adipose tissue of male (D/D) mice and the epididymal adipose tissue of (R/D) and (R/R) mice are indicated by arrows.

(E) Quantification of the fat tissue mass of the epididymal (R/R and R/D) and dorsal (D/D) white adipose tissues.  $n = 5$  for (D/D), (R/R), and their littermate control groups. Each group contains both males and females. The gender ratio between control and experimental groups is matched.  $n = 4$  for (R/D) and their littermate control mice.  $\pm$  SEM,  $*p = 0.0159$ ,  $**p = 0.0579$ ,  $***p = 0.0079$ . Mann-Whitney U test.

(F) Frontal views of the lumbar spine of micro-computed tomography X-ray analysis of mice with indicated genotypes and ages. Mild reduction in the height of vertebrae is observed in (R/D) and (D/D) mice. Scale bar, 1 mm.

of the vertebral bodies, and slender diaphyses and relatively wide metaphyses of tubular bones (Figure 1A). The patient died at the age of 2 years and 7 months after developing pneumonia and respiratory failure. Autopsy revealed mild deformity of vertebral bodies and relatively prominent retroperitoneal brown adipose tissues (Figure 1B). Histological analysis showed microvesicular steatosis in the liver (Figure 1C) and relatively small white adipocytes in the retroperitoneal fat tissue (Figure 1D). In addition to diffuse bilateral pneumonia, there were also submucosal fibrosis of the intestine, smooth muscle degeneration of the rectum, and thickening of the tunica intima and edema and proteoglycan deposition in the tunica media of the aorta and coronary arteries, but the clinical significance of these findings was unclear (Figure S1).

The initial analysis of whole genome sequencing (WGS) of this affected individual and his parents did not reveal

any candidate variants in all known skeletal dysplasia genes (<https://panelapp.genomicsengland.co.uk/panels/309/>). Extended analysis revealed several possible candidate variants (Table S3) including a single-nucleotide substitution in the TOMM7 gene (chr7:g.22862326T>C (hg19), NM\_019059.5 (TOMM7):c.73T>C, p.(Trp25Arg)). This variant was found in the homozygous state in the affected individual and in the heterozygous state in his parents (Figure 1E). The tryptophan at the position 25 of TOMM7, located at a kinked region, is highly conserved across many species (Figure 1F). This variant is expected to replace the tryptophan residue with a positively charged arginine located next to another arginine at the position 24. It is reported that the position 24 arginine is important for the interaction between TOMM7 and -40 barrel.<sup>20</sup> Thus, we hypothesized that the Trp25Arg (W25R) variant interfered with the normal interaction between TOMM7

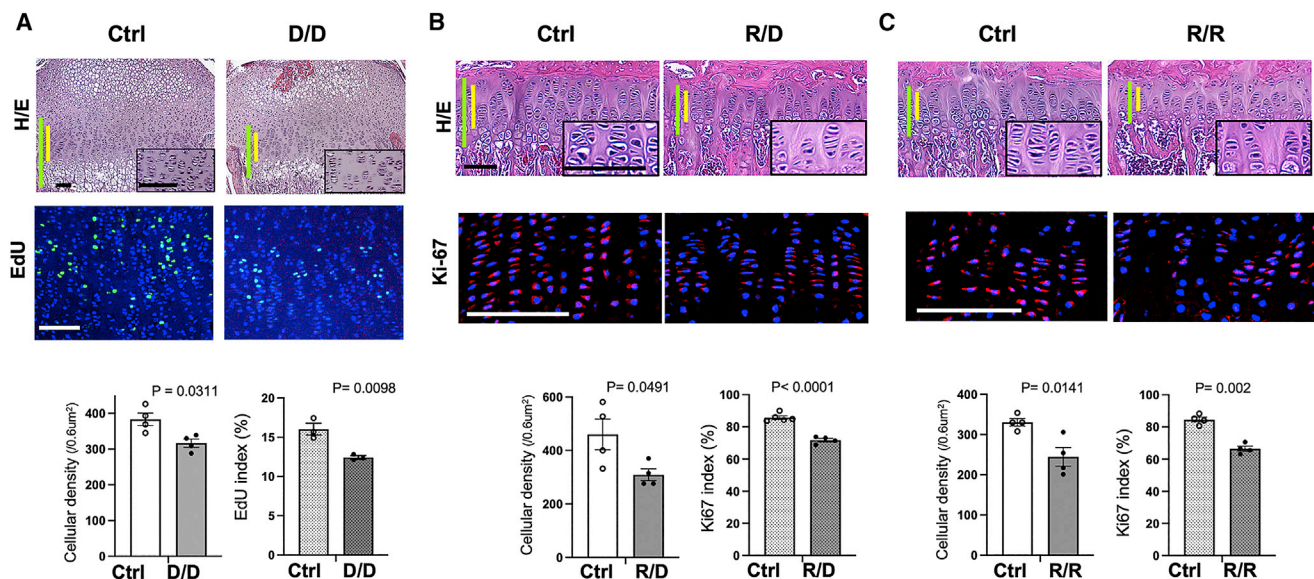


**Figure 3. Hypocellularity and reduced proliferation in the mutant growth plates**

(A) Tibial growth plates of P15 *Tomm7(D/D)* mice and control littermates. Hematoxylin and eosin (H&E)-stained sections (top). The insets are magnified views of the proliferating zone (indicated by yellow bar) of the growth plate (green bar). Quantification of the cellular density and EdU index of the proliferating zone are shown (middle and bottom).  $\pm$  SEM,  $n = 3$ , t test.

(B) Tibial growth plates of P40 *Tomm7(R/D)* mice and control littermates. H&E-stained sections (top). The insets are magnified views of the proliferating zone (yellow bar) of the growth plate (green bar). Quantification of the cellular density and Ki67 index of the proliferating zone are shown (middle and bottom).  $\pm$  SEM,  $n = 4-5$ , t test.

(C) Tibial growth plates of P61 *Tomm7(R/R)* mice and control littermates. H&E-stained sections (top). The insets are magnified views of the proliferating zone (yellow bar) of the growth plate (green bar). Quantification of the cellular density and Ki67 index of the proliferating zone are shown (middle and bottom).  $\pm$  SEM,  $n = 4$ , t test. Scale bar, 100  $\mu$ m.

and -40, leading to pathogenic consequences. To test this hypothesis, we generated a knockin mouse model where the identical amino acid variant (W25R) was introduced to the mouse *Tomm7* gene. We also generated a mouse line missing a 184 bp genomic region spanning the first exon-intron boundary of the *Tomm7* gene (deletion [D]) (Figure 2A). The D allele is expected to be functionally null because the deletion leads to a disruption of normal splicing resulting in premature termination. This deletion also caused a substantial reduction of *Tomm7* transcripts, likely due to a nonsense-mediated decay-like mechanism,<sup>23</sup> whereas *Tomm7(R/R)* cells expressed a comparable amount of *Tomm7* RNA as wild-type cells (Figure 2B).

Mice heterozygous for the D or R allele are grossly normal and indistinguishable from wild-type littermates. Homozygous *Tomm7(R/R)* mice showed relatively normal growth up to 7–8 weeks, but then they developed rapidly progressing emaciation leading to sudden death at around 9 to 10 weeks of age (Figure 2C). On the other hand, *Tomm7(D/D)* mice showed a significant growth failure in early postnatal stages, followed by death at 3 to 4 weeks of age after rapid weight loss near the end of their lives (Figure 2C). This phenotype is similar to that of previously reported *Tomm7* knockout mice.<sup>24</sup> Compound heterozygotes, *Tomm7(R/D)* mice showed relatively normal growth but again developed rapid weight loss around 5–6 weeks and died by 6–7 weeks (Figure 2C). These observations support the notion that the missense variant causes partial loss

of *Tomm7* function. The most prominent gross phenotype in these mouse models is lipoatrophy (Figures 2D and 2E). Since OXPHOS defects cause tissue-autonomous lipoatrophy,<sup>25,26</sup> these findings suggest that *Tomm7* deficiency impairs mitochondrial bioenergetics.

Growth failure and mild spondyloepimetaphyseal dysplasia features have been previously described in mitochondrial diseases.<sup>27–33</sup> Variants in several genes encoding proteins regulating mitochondrial protein homeostasis, including *TOMM70*,<sup>34</sup> have been reported to associate with skeletal abnormalities. To characterize the skeletal phenotype of these mouse models, we performed micro-computed tomography ( $\mu$ CT) and histological analyses. The  $\mu$ CT images of the spine revealed a modest shortening of vertebral bodies in *Tomm7(R/D)* and *Tomm7(D/D)* mice, reminiscent of the platyspondyly detected in the patient (Figures 2F and S2). The longitudinal growth of vertebral bodies and appendicular bones is driven by the growth plate. To investigate the abnormalities in growth plate cartilage, we analyzed the tibial growth plates that are much larger than those of vertebral bodies. Histological analysis of tibial growth plates of mutant mice showed a shortening of the growth plate with reduced cellular densities and cellular proliferation, assessed by EdU labeling in young mice and with Ki-67 staining in older mice (Figures 3A–3C), suggesting that the reduced chondrocyte proliferation contributes to the skeletal phenotype. Similar changes were also found in *Tomm7(R/R)* mice that showed

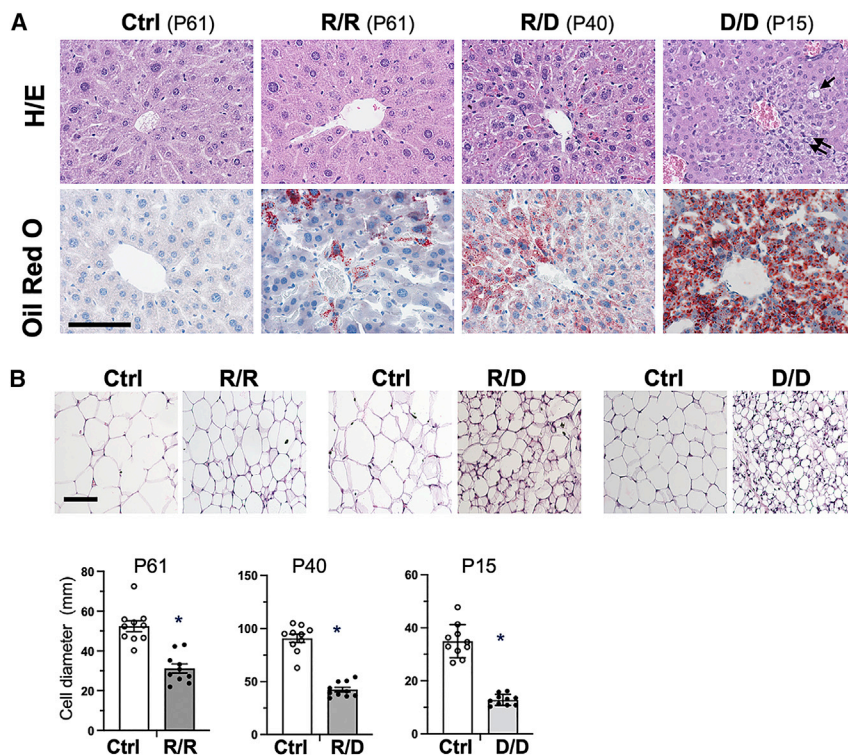


**Figure 4. Lipid accumulation in the liver and peripheral fat loss in mutant mice**

(A) The liver tissues from mice with indicated genotypes and ages. H&E staining of paraffin-processed sections (top) and oil red O staining of frozen sections (bottom). Arrows indicate cytoplasmic vacuoles in hepatocytes, suggesting lipid accumulation. Scale bar, 100  $\mu$ m.

(B) H&E sections of epididymal (R/R and R/D) and dorsal (D/D) white adipose tissues (top) and quantification of adipocyte diameter. The maximal length of the longitudinal axis of cross sections of adipocytes was counted in 10 randomly selected cells per group. Scale bar, 100  $\mu$ m.  $\pm$  SEM,  $n = 10$ , \*  $p < 0.0001$ , t-test

only a modest growth defect. Additionally, these results suggest that the normal mitochondrial function plays an important regulatory role in growth plate chondrocytes, which predominantly rely on glycolysis, rather than mitochondrial metabolism, for ATP synthesis.<sup>35</sup> Additional histological assessment of *Tomm7* mutant tissues showed lipid accumulation in the liver (Figure 4A) and reductions in size of adipocytes (Figure 4B), findings observed also in the patient and consistent with mitochondrial dysfunction.<sup>13,15,20</sup>

These data provide evidence that the TOMM7 W25R variant found in the affected individual is pathogenic and causes mitochondrial dysfunction at the organismal and tissue levels. This notion is also supported by the fact that this patient presents findings frequently observed in mitochondrial diseases, including hypotonia, nystagmus, elevated LDH levels, and fat accumulation in the liver. At subcellular and molecular levels, *Tomm7* deficiency does not appear to significantly affect mitochondrial morphology except that mutant mitochondria in muscle appear generally small in size and that mild structural changes may develop in older mice (Figures 5A and S3–S5), whereas tissue expression of *Gdf15* and *Fgf21*, markers for mitochondrial dysfunction<sup>36</sup> were significantly upregulated in both *Tomm7(D/D)* and *Tomm7(R/R)* tissues (Figure 5B).

As expected from the mouse phenotype, phosphorylation of AMP-dependent protein kinase (AMPK), a pivotal energy sensor in the cell,<sup>37</sup> was upregulated in multiple tissues of *Tomm7* mutants, indicating inefficient ATP synthesis in mutant cells (Figure 5C). Interestingly, multiple types of

*Tomm7*-deficient cells showed increases not only in extracellular acidification rate (ECAR) but also in oxygen consumption rate (OCR) and showed normal responses to inhibitors of the electron transport chain (ETC) and ATP synthase (complex V) (Figures 5D and S6). These results suggest that the function of ETC and the proton transportation of ATP synthase are maintained intact in *Tomm7*-deficient cells (Figure 5D). Similar to *Tomm7(D/D)* cells, the upregulation in both OCR and ECAR was also observed in *Tomm7(R/R)* cells (Figure S7). Flow cytometric analysis showed a slight increase in membrane potential, as assessed by TMRE staining in *Tomm7(D/D)* chondrocyte samples, whereas the mitochondrial mass, assessed by MitoTracker staining, was modestly reduced (Figure 5E). Unlike in a previous zebrafish study,<sup>24</sup> we did not find significant changes in reactive oxygen species (ROS), as assessed by MitoSox staining. These findings may reflect the hyperactive state of the ETC. These changes were generally found also in other cell types of *Tomm7(D/D)* cells (Figure S8) and were partially found in *Tomm7(R/R)* cells (Figure S9).

The upregulation both in OCR and in ECAR despite the increase in p-AMPK suggests that there is a dissociation between oxidation and ATP synthesis in *Tomm7* mutant mitochondria. Such uncoupling is physiologically observed in brown adipose tissues where uncoupling protein 1 (*Ucp1*)<sup>38</sup> mediates the effect. We analyzed the expression of *Ucp1* and its paralogs, *Ucp2* and *Ucp3*,<sup>39</sup> in primary bone marrow stromal cells (BMSCs) and in the brain of *Tomm7(D/D)* mice. We found that these genes were generally downregulated rather than upregulated except for a modest upregulation of *Ucp3* in the brain, suggesting that aberrant uncoupling protein expression is an unlikely mechanism for the impaired ATP synthesis in *Tomm7* mutant cells (Figure S10). ATP deficiency can be caused by defects in transport of ATP generated in the mitochondrial matrix into the cytoplasm, which is mediated by adenine nucleotide translocase (ANT)

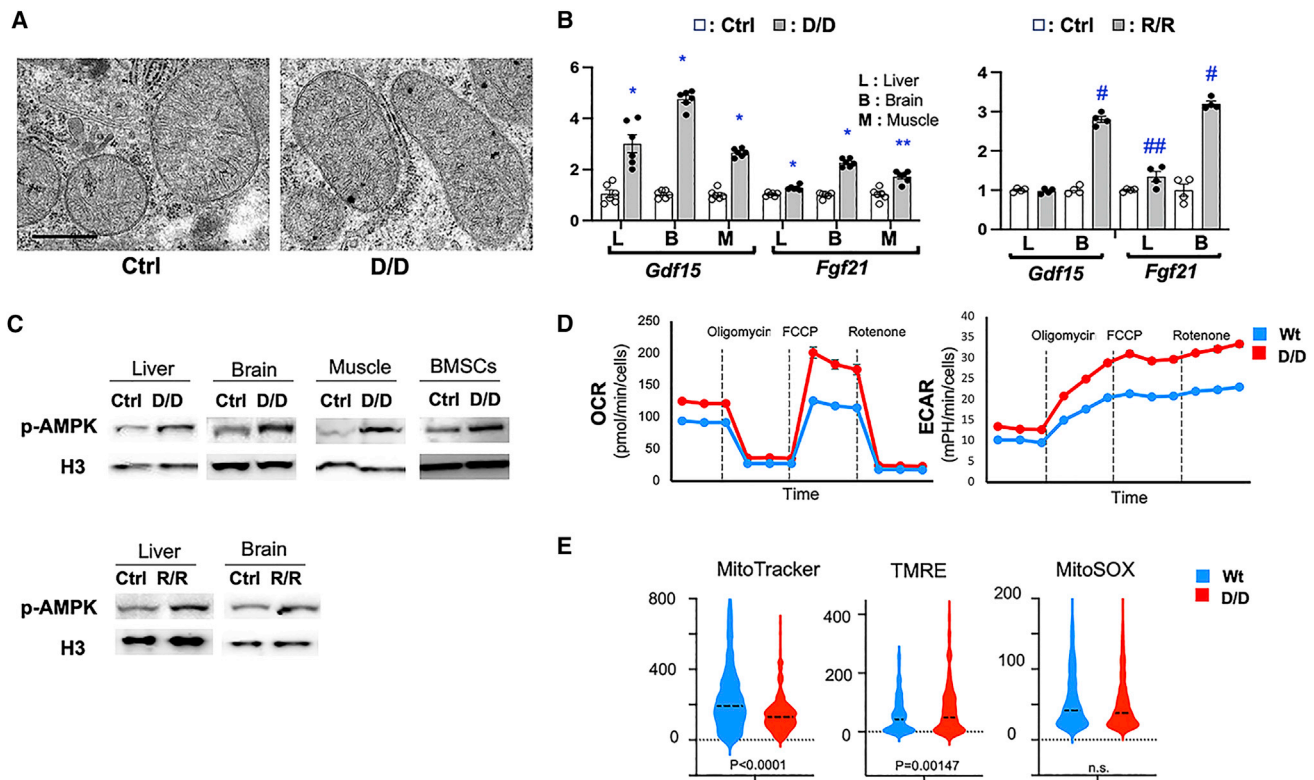


**Figure 5. Altered mitochondrial function in mutant mice**

(A) Representative transmission electron microscope images of liver mitochondria in hepatocytes of P15 *Tomm7(D/D)* mice and control littermates (30,000 $\times$ ). Scale bar, 600 nm.

(B) mRNA expression of markers for mitochondrial dysfunction, *Gdf15* and *Fgf21*, in indicated tissues. Significant upregulation of these markers was observed in both in *Tomm7(D/D)* and *Tomm7(R/R)* tissues.  $n = 4 - 6$ ,  $\pm$  SEM, \*  $p = 0.0022$ , \*\*  $p = 0.0043$ , #  $p = 0.0286$ , ##  $p = 0.0571$  vs Ctrl, Mann-Whitney U test.

(C) Upregulation of phospho-AMPK expression in indicated tissues.

(D) Seahorse analysis using primary rib chondrocytes of *Tomm7(D/D)* and littermate control mice. Oxygen consumption rate (OCR) and extracellular acidification rate (ECAR) were measured at the basal level and upon treatment with the ATP synthase inhibitor, oligomycin, the uncoupler, FCCP, and the ETC inhibitor, rotenone, and antimycin A (Rotenone). Both OCR and ECAR are significantly upregulated. Mean  $\pm$  SEM.  $n = 8$ ,  $p < 0.001$  at all data points. t test.

(E) Flow cytometric analysis of primary rib chondrocytes. Cells were pre-incubated with the indicated fluorescent dyes and subjected to flow cytometric analysis. The signal intensity of 500 randomly selected cells per group was evaluated. Dotted lines indicate median values. Mitochondrial membrane potential (TMRE) is slightly upregulated in *Tomm7(D/D)* despite the decreased mitochondrial mass (MitoTracker).

family proteins and voltage-dependent anion channels (VDACs).<sup>40,41</sup> We examined the expression of *Slc25a2*, a major ANT, and *Vdac1*, a major VDAC, in mitochondria-enriched protein fractions of *Tomm7(D/D)* mice; however, we did not find significant changes in their abundance (Figure S11). The bioenergetic dysfunction and the increased oxygen consumption with normal response to oligomycin, a proton transport inhibitor of complex V, suggest that there is a dissociation between proton transport and catalytic activity of complex V. Complex V consists of two rotary motors, the membrane-bound  $F_0$  that mediates proton transport and  $F_1$  that is responsible for ATP synthesis. We assessed the expression of several complex V subunits along with ETC subunits, but we did not find overt changes in the abundance of these proteins, suggesting that *Tomm7* deficiency may have relatively limited impact on mitochondrial proteostasis (Figure S11). Independently of the mitochondrial bioenergetic dysfunction, it could be possible that *Tomm7* deficiency contributes to

the phenotype via suppressing PINK1/parkin-mediated mitophagy. We have tested whether *Tomm7* deficiency alters PINK1 expression using primary mouse BMSCs. Upon mitochondrial stress, PINK1 expression was induced both in control and in *Tomm7*-deficient cells to similar extents. This finding suggests that *Tomm7*'s regulatory role in PINK1 expression in mouse skeletal progenitors is limited (Figure S12).

In summary, this study identifies *TOMM7* as a new human disease gene and provides genetic evidence that this variant is pathogenic and creates a hypomorphic allele. This study presents evidence that aberration of mitochondrial protein homeostasis leads to mitochondrial disease with skeletal involvement, as previously suggested by several reports.<sup>42</sup> *Tomm7* deficiency in mice results in a phenotype consistent with mitochondrial bioenergetic deficiency, yet *Tomm7*-deficient cells show increased oxygen consumption with normal responses to ETC and ATP synthase inhibitors, suggesting that *Tomm7* deficiency

does not impair the function of the tricarboxylic cycle, ETC, or proton transport by the complex V. These data suggest a discordance between proton transport ( $F_0$ ) and catalytic function of ATP synthase ( $F_1$ ). However, we did not find overt changes in the stoichiometry of some of complex V subunits; the precise mechanism by which Tom7 deficiency causes dysfunction in ATP synthesis is currently unclear.

### Data availability

The variant has been submitted to the ClinVar database (accession number SCV002505631).

### Supplemental information

Supplemental information can be found online at <https://doi.org/10.1016/j.xhgg.2022.100148>.

### Acknowledgments

We thank the Center for Skeletal Research (P30AR075042) for assistance in histological analysis. We thank Dr. Patrick Ward and Dr. Lawrence Zukerberg for valuable comments on mitochondrial biology and liver pathology. This study was supported by the NIH grant ARO56645 (T.K.) and by grants from Stiftelsen Samartiten, Stiftelsen Promobilia, and Stiftelsen Frimurare Barnhuset i Stockholm, Stiftelsen Sällsntafonden, from Region Stockholm (20180131 and 20200500), from Swedish Research Council (2018-03046), and by the Karolinska Institutet (G.G. and D.B.).

### Declaration of interests

The authors declare no competing interests.

Received: May 23, 2022

Accepted: September 29, 2022

### Web resources

CADD, <https://cadd.gs.washington.edu/>.

ClinVar, <https://www.ncbi.nlm.nih.gov/clinvar/>.

DECIPHER, <https://www.deciphergenomics.org/>.

Genomics England PannelApp, <https://panelapp.genomicsengland.co.uk/#!>.

OMIM, <https://omim.org/>.

### References

- Wallace, D.C. (2012). Mitochondria and cancer. *Nat. Rev. Cancer* 12, 685–698.
- Moos, W.H., Faller, D.V., Glavas, I.P., Harpp, D.N., Kamperi, N., Kanara, I., Kodukula, K., Mavrakis, A.N., Pernokas, J., Pernokas, M., et al. (2021). Pathogenic mitochondrial dysfunction and metabolic abnormalities. *Biochem. Pharmacol.* 193, 114809.
- Rey, F., Ottolenghi, S., Zuccotti, G.V., Samaja, M., and Carelli, S. (2022). Mitochondrial dysfunctions in neurodegenerative diseases: role in disease pathogenesis, strategies for analysis and therapeutic prospects. *Neural Regen. Res.* 17, 754–758.
- Forbes, J.M., and Thorburn, D.R. (2018). Mitochondrial dysfunction in diabetic kidney disease. *Nat. Rev. Nephrol.* 14, 291–312.
- Salnikova, D., Orekhova, V., Grechko, A., Starodubova, A., Bezsonov, E., Popkova, T., and Orekhov, A. (2021). Mitochondrial dysfunction in vascular wall cells and its role in atherosclerosis. *Int. J. Mol. Sci.* 22, 8990.
- Jankovic, M., Novakovic, I., Gamil Anwar Dawod, P., Gamil Anwar Dawod, A., Drinic, A., Abdel Motaleb, F.I., Ducic, S., and Nikolic, D. (2021). Current concepts on genetic aspects of mitochondrial dysfunction in amyotrophic lateral sclerosis. *Int. J. Mol. Sci.* 22, 9832.
- DiMauro, S. (2004). Mitochondrial diseases. *Biochim. Biophys. Acta* 1658, 80–88.
- Gorman, G.S., Chinnery, P.F., DiMauro, S., Hirano, M., Koga, Y., McFarland, R., Suomalainen, A., Thorburn, D.R., Zeviani, M., and Turnbull, D.M. (2016). Mitochondrial diseases. *Nat. Rev. Dis. Primers* 2, 16080.
- Cotter, D., Guda, P., Fahy, E., and Subramaniam, S. (2004). MitoProteome: mitochondrial protein sequence database and annotation system. *Nucleic Acids Res.* 32, D463–D467.
- Chacinska, A., Koehler, C.M., Milenkovic, D., Lithgow, T., and Pfanner, N. (2009). Importing mitochondrial proteins: machineries and mechanisms. *Cell* 138, 628–644.
- Moehle, E.A., Shen, K., and Dillin, A. (2019). Mitochondrial proteostasis in the context of cellular and organismal health and aging. *J. Biol. Chem.* 294, 5396–5407.
- Araiso, Y., Imai, K., and Endo, T. (2021). Structural snapshot of the mitochondrial protein import gate. *FEBS J.* 288, 5300–5310.
- Yamano, K., Tanaka-Yamano, S., and Endo, T. (2010). Tom7 regulates Mdm10-mediated assembly of the mitochondrial import channel protein Tom40. *J. Biol. Chem.* 285, 41222–41231.
- Bausewein, T., Mills, D.J., Langer, J.D., Nitschke, B., Nussberger, S., and Kühlbrandt, W. (2017). Cryo-EM structure of the TOM core complex from *Neurospora crassa*. *Cell* 170, 693–700.e7.
- Wiedemann, N., Kozjak, V., Chacinska, A., Schönfisch, B., Rospert, S., Ryan, M.T., Pfanner, N., and Meisinger, C. (2003). Machinery for protein sorting and assembly in the mitochondrial outer membrane. *Nature* 424, 565–571.
- Dembowski, M., Kunkele, K.P., Nargang, F.E., Neupert, W., and Rapaport, D. (2001). Assembly of Tom6 and Tom7 into the TOM core complex of *Neurospora crassa*. *J. Biol. Chem.* 276, 17679–17685.
- Pfanner, N., Wiedemann, N., Meisinger, C., and Lithgow, T. (2004). Assembling the mitochondrial outer membrane. *Nat. Struct. Mol. Biol.* 11, 1044–1048.
- Hasson, S.A., Kane, L.A., Yamano, K., Huang, C.H., Sliter, D.A., Buehler, E., Wang, C., Heman-Ackah, S.M., Hessa, T., Guha, R., et al. (2013). High-content genome-wide RNAi screens identify regulators of parkin upstream of mitophagy. *Nature* 504, 291–295.
- Sekine, S., Wang, C., Sideris, D.P., Bunker, E., Zhang, Z., and Youle, R.J. (2019). Reciprocal roles of Tom7 and OMA1 during mitochondrial import and activation of PINK1. *Mol. Cell* 73, 1028–1043.e5.
- Wang, W., Chen, X., Zhang, L., Yi, J., Ma, Q., Yin, J., Zhuo, W., Gu, J., and Yang, M. (2020). Atomic structure of human TOM core complex. *Cell Discov.* 6, 67.
- Wang, Y., Adress, K.J., Chen, J., Geer, L.Y., He, J., He, S., Lu, S., Madej, T., Marchler-Bauer, A., Thiessen, P.A., et al. (2007).

- MMDB: annotating protein sequences with Entrez's 3D-structure database. *Nucleic Acids Res.* 35, D298–D300.
22. Sayers, E.W., Bolton, E.E., Brister, J.R., Canese, K., Chan, J., Coomeau, D.C., Connor, R., Funk, K., Kelly, C., Kim, S., et al. (2022). Database resources of the national center for biotechnology information. *Nucleic Acids Res.* 50, D20–D26.
  23. Brogna, S., and Wen, J. (2009). Nonsense-mediated mRNA decay (NMD) mechanisms. *Nat. Struct. Mol. Biol.* 16, 107–113.
  24. Shi, D., Qi, M., Zhou, L., Li, X., Ni, L., Li, C., Yuan, T., Wang, Y., Chen, Y., Hu, C., et al. (2018). Endothelial mitochondrial pre-protein translocase Tomm7-Rac1 signaling axis dominates cerebrovascular network homeostasis. *Arterioscler. Thromb. Vasc. Biol.* 38, 2665–2677.
  25. Vernochet, C., Mourier, A., Bezy, O., Macotela, Y., Boucher, J., Rardin, M.J., An, D., Lee, K.Y., Ilkayeva, O.R., Zingaretti, C.M., et al. (2012). Adipose-specific deletion of TFAM increases mitochondrial oxidation and protects mice against obesity and insulin resistance. *Cell Metab.* 16, 765–776.
  26. Vernochet, C., Damilano, F., Mourier, A., Bezy, O., Mori, M.A., Smyth, G., Rosenzweig, A., Larsson, N.G., and Kahn, C.R. (2014). Adipose tissue mitochondrial dysfunction triggers a lipodystrophic syndrome with insulin resistance, hepatosteatosis, and cardiovascular complications. *FASEB J.* 28, 4408–4419.
  27. Boal, R.L., Ng, Y.S., Pickett, S.J., Schaefer, A.M., Feeney, C., Bright, A., Taylor, R.W., Turnbull, D.M., Gorman, G.S., Cheetham, T., and McFarland, R. (2019). Height as a clinical biomarker of disease burden in adult mitochondrial disease. *J. Clin. Endocrinol. Metab.* 104, 2057–2066.
  28. Castro-Gago, M., Gómez-Lado, C., Pérez-Gay, L., and Eirís-Puñal, J. (2010). Abnormal growth in mitochondrial disease. *Acta Paediatr.* 99, 796.
  29. Jabbour, S., and Harissi-Dagher, M. (2016). Recessive mutation in a nuclear-encoded mitochondrial tRNA synthetase associated with infantile cataract, congenital neurotrophic keratitis, and orbital myopathy. *Cornea* 35, 894–896.
  30. Mierzevska, H., Rydzanicz, M., Biegański, T., Kosinska, J., Mierzevska-Schmidt, M., Ługowska, A., Pollak, A., Stawiński, P., Walczak, A., Kędra, A., et al. (2017). Spondyloepimetaphyseal dysplasia with neurodegeneration associated with AIFM1 mutation - a novel phenotype of the mitochondrial disease. *Clin. Genet.* 91, 30–37.
  31. Vona, B., Maroofian, R., Bellacchio, E., Najafi, M., Thompson, K., Alahmad, A., He, L., Ahangari, N., Rad, A., Shahrokhzadeh, S., et al. (2018). Expanding the clinical phenotype of IARS2-related mitochondrial disease. *BMC Med. Genet.* 19, 196.
  32. Wolny, S., McFarland, R., Chinnery, P., and Cheetham, T. (2009). Abnormal growth in mitochondrial disease. *Acta Paediatr.* 98, 553–554.
  33. Zhao, T., Goedhart, C.M., Sam, P.N., Sabouny, R., Lingrell, S., Cornish, A.J., Lamont, R.E., Bernier, F.P., Sinasac, D., Parboosingh, J.S., et al. (2019). PISD is a mitochondrial disease gene causing skeletal dysplasia, cataracts, and white matter changes. *Life Sci Alliance* 2, e201900353.
  34. Wei, X., Du, M., Xie, J., Luo, T., Zhou, Y., Zhang, K., Li, J., Chen, D., Xu, P., Jia, M., et al. (2020). Mutations in TOMM70 lead to multi-OXPHOS deficiencies and cause severe anemia, lactic acidosis, and developmental delay. *J. Hum. Genet.* 65, 231–240.
  35. Stegen, S., Laperre, K., Eelen, G., Rinaldi, G., Fraisl, P., Torrekens, S., Van Looveren, R., Loopmans, S., Bultynck, G., Vinckier, S., et al. (2019). HIF-1 $\alpha$  metabolically controls collagen synthesis and modification in chondrocytes. *Nature* 565, 511–515.
  36. Maresca, A., Del Dotto, V., Romagnoli, M., La Morgia, C., Di Vito, L., Capristo, M., Valentino, M.L., Carelli, V.; and ER-MITO Study Group (2020). Expanding and validating the biomarkers for mitochondrial diseases. *J. Mol. Med.* 98, 1467–1478.
  37. Herzig, S., and Shaw, R.J. (2018). AMPK: guardian of metabolism and mitochondrial homeostasis. *Nat. Rev. Mol. Cell Biol.* 19, 121–135.
  38. Kalinovich, A.V., de Jong, J.M.A., Cannon, B., and Nedergaard, J. (2017). UCP1 in adipose tissues: two steps to full browning. *Biochimie* 134, 127–137.
  39. Nicholls, D.G. (2021). Mitochondrial proton leaks and uncoupling proteins. *Biochim. Biophys. Acta. Bioenerg.* 1862, 148428.
  40. Ruprecht, J.J., King, M.S., Zögg, T., Aleksandrova, A.A., Pardon, E., Crichton, P.G., Steyaert, J., and Kunji, E.R.S. (2019). The molecular mechanism of transport by the mitochondrial ADP/ATP carrier. *Cell* 176, 435–447.e15.
  41. Heslop, K.A., Milesi, V., and Maldonado, E.N. (2021). VDAC modulation of cancer metabolism: advances and therapeutic challenges. *Front. Physiol.* 12, 742839.
  42. Zhao, T., Goedhart, C., Pfeffer, G., Greenway, S.C., Lines, M., Khan, A., Innes, A.M., and Shutt, T.E. (2020). Skeletal phenotypes due to abnormalities in mitochondrial protein homeostasis and import. *Int. J. Mol. Sci.* 21, E8327.